Application of a Dynamic Pressure-Sinkage Relationship for Lightweight Mobile Robots

Rishad A. Irani*

Dalhousie University,
Department of Mechanical Engineering
Halifax, Nova Scotia B3J 1Z1, Canada
E-mail: rirani@dal.ca
*Corresponding author

Robert J. Bauer

Dalhousie University,
Department of Mechanical Engineering
Halifax, Nova Scotia B3J 1Z1, Canada
E-mail: robert.bauer@dal.ca

Andrew Warkentin

Dalhousie University,
Department of Mechanical Engineering
Halifax, Nova Scotia B3J 1Z1, Canada
E-mail: andrew.warkentin@dal.ca

Abstract: This paper investigates a dynamic pressure-sinkage relationship which can be used in a wheel-soil model to better capture periodic variations observed in sinkage, drawbar pull and normal force as a rigid wheel interacts with loose sandy soil. The dynamic wheel-soil model can be used for wheels with or without grousers. Several case studies are presented to demonstrate the usefulness and applicability of this dynamic pressure-sinkage relationship. Hill climbing experiments were carried out using a smooth-wheel micro rover with a fixed suspension to confirm operational regions of the dynamic pressure-sinkage relationship. Single wheel testbed experiments were carried out to determine how well the model can predict changes in the number and length of the grousers on the wheel. It was concluded that dynamic pressure-sinkage relationship can predict the observed oscillations in the sinkage, drawbar pull and normal force with a single tuning case as the slip ratio and the configuration of the wheel changes.

Keywords: Terramechanics; Sandy Soil Modeling; Pressure-Sinkage Relationship; Rigid Wheel; Grousers

Biographical notes: Rishad Irani completed his BASc at the University of Windsor in 2003 and his MASc at Dalhousie University in 2006. Rishad completed his PhD in 2011 by examining the mobility issues that face the next generation of Mars Rovers under the supervision of Dr. Robert Bauer. Robert J. Bauer received a BASc in

Mechanical Engineering from the University of Waterloo in 1994. In 1998, he received a PhD in Aerospace Engineering from the University of Toronto. In 1998, he joined the Mechanical Engineering faculty at Dalhousie University and is currently a Professor carrying out research in process modeling and control of dynamic systems. Andrew

Warkentin completed his Bachelor's degree in 1991 and Master's degree in 1993 at McMaster University and went on to complete a PhD at the University of Waterloo in 1997. He continued his research at Waterloo with an NSERC Post-Doctoral Fellowship. In 1998, he joined Dalhousie University where he teaches Design and Manufacturing in the Department of Mechanical Engineering.

In the past few years there has been a considerable amount of research involving lightweight mobile robots — specifically, planetary rovers. Much of this work stems from several planetary exploratory missions by various agencies including National Aeronautics and Space Administration (NASA), the European Space Agency (ESA) and Japan Aerospace Exploration Agency (JAXA). There has even been mobilization in the private sector for planetary rovers and several official teams which are privately funded and competing in the Google Lunar X PRIZE competition.

To enhance the mobility of any of these lightweight planetary rovers or exploratory vehicles a high fidelity wheel-soil interaction model is needed. Typically, empirically-based static or quasi-static models are used for these low-speed applications. Lyasko (2010) reported that the most common formulation for the wheel-soil interaction with rigid wheels is based on the work of Bekker (1969), which is a semi-empirical quasi-static model. Despite the significant research to develop wheel-soil interaction models, Azimi et al. (2010) concluded that there is still a need for further validation and improvement of the traditional semi-empirical quasi-static terramechanic model of Bekker (1969) and Wong (2010). Irani et al. (2010a) introduced a dynamic wheel-soil interaction model which advances classic work by Bekker and Wong, such that the oscillations about the predicted or modeled drawbar pull can now be represented for a smooth rigid wheel. Irani et al. (2011a) used Reece's (1965) pressure-sinkage relationship to advance their own model and presented a terramechanic model which focuses on predicting the oscillations in the drawbar pull, normal force and sinkage for lightweight vehicles for a wheel with grousers.

This paper presents a series of case studies using the more advanced semi-empirical dynamic terramechanic model which was developed by Irani et al. (2011a). The work presented here will feature case studies to show how the model can be used to accurately predict the fluctuations in the measured data of the wheel-soil interaction for a rigid wheel operating in sandy soil with and without grousers. Figure 1 shows a sample of these oscillations observed in the measured data from a single-wheel testbed for a 200mm diameter rigid wheel with 16, 23mm long grousers operating at a slip ratio of 0.50. It will also be shown that the model is able to predict these fluctuations as the slip ratio and the configuration of the grouser wheel changes with no re-calibration of the model.

1 Terramechanic Model

Figure 2 shows the forces and stresses which need to be calculated so that they can be used to determine the trafficability, motion planning and/or control algorithms for the full vehicle. The classic terramechanic model for a smooth rigid wheel described by Bekker (1969) assumes that the pressure p under a wheel can be approximated by a flat plate with an exponential function as follows:

$$p\left(z\right) = \left(\frac{k_c}{b} + k_\phi\right) z^n \tag{1}$$

where z is the instantaneous sinkage, n is the sinkage exponent, b is the smaller dimension of the wheels contact patch and k_c and k_ϕ are an empirical coefficients which are found though infield bevameter testing (Bekker (1969)). Reece (1965) proposed that the pressure-sinkage relationship can also be expressed as a function of two dimensionless coefficients k'_c and k'_ϕ, the wheel sinkage z and wheel width b, such that:

$$p\left(z\right) = \left(ck'_c + \gamma bk'_\phi\right)\left(\frac{z}{b}\right)^n \tag{2}$$

Here, c and γ are the terrain's cohesion and weight density respectively and k'_c and k'_ϕ can be tuned to the specific terrain and operating conditions. The dynamic model proposed by Irani et al. (2011a) uses the Reece pressure-sinkage relationship to estimate the oscillations seen in the sinkage, drawbar pull and normal load. The dynamic pressure-sinkage relationship has the general form:

$$p(z) = \left(ck'_c + \gamma bk'_\phi\right)\left(\frac{z}{b}\right)^n + A\sin\left(\omega t + \Phi\right) \tag{3}$$

where t is time and Φ is an optional phase shift that can be applied to the model for fitting the simulation predictions to experimental data or applying a correction to account for the initial orientation of the grousers. The A term is the amplitude of the oscillations and ω is the frequency at which they occur. The traditional terramechanic model will estimate the average normal stress by a curve governed by Equation (1) which does not explicitly account for the wheel geometry in the classic terramechanic model. Karafiath and Nowatzki (1978) proposed that the normal stress distribution is not a smooth curve but rather is a discontinuous function as the grousers will affect the stresses acting on the terrain. Irani et al. (2011a) has shown that the dynamic model is able to estimate the fluctuations and variations in the pressure-sinkage relationship that is caused by the presence of grousers which Karafiath and Nowatzki hypothesized.

The modified Mohr Coulomb failure criteria developed by Janosi and Hanamoto (1961) can be used to determine the shear stress τ acting along the wheel-soil interface such that:

$$\tau\left(\theta\right) = \left(c + \sigma\left(\theta\right)\tan\phi\right)\left[1 - e^{-j(\theta)/K}\right] \tag{4}$$

where θ angular location of the wheel-soil interface, ϕ is the internal angle of friction, K is a soil property known as the shear deformation modulus, and j has the form:

$$j(\theta) = r\left[\theta_f - \theta - (1-i)(\sin\theta_f - \sin\theta)\right] \tag{5}$$

The slip ratio i for this work is defined as:

$$i = \frac{\omega_w r - V_x}{\omega_w r} \tag{6}$$

where ω_w is the angular velocity of the wheel, r is the radius of the wheel, and V_x is the translational velocity of the wheel centre.

Converting $p(z)$ to polar coordinates, the pressure becomes the normal stress $\sigma(\theta)$ as shown in Figure 2 and shear stress $\tau(\theta)$ can be calculated by Equation (4) in the wheel-soil interaction. The vertical force F_z is calculated by taking the area integrals of the stresses in the vertical direction and the drawbar pull DP is computed by the area integrals of the stresses in the horizontal direction, such that:

$$F_z = rb\int_{\theta_r}^{\theta_f} \left(\tau(\theta)\sin\theta + \sigma(\theta)\cos\theta\right) d\theta \tag{7}$$

$$DP = F_x = rb\int_{\theta_r}^{\theta_f} \left(\tau(\theta)\cos\theta - \sigma(\theta)\sin\theta\right) d\theta \tag{8}$$

The entry and departure angles, θ_f and θ_r, of the wheel-soil interface are calculated by:

$$\theta_f = \cos^{-1}(1 - z/r) \tag{9}$$

$$\theta_r = -\cos^{-1}(1 - \eta z/r) \tag{10}$$

where η, also shown in Figure 2, is a dimensionless empirical parameter which compares the nominal wheel sinkage z to the depth of the track left by the wheel. Ishigami et al. (2007) states that η is related to the soil properties, slip ratio and the wheel surface pattern.

If one uses the Reece pressure sinkage relationship shown in Equation (2), then the resulting calculated drawbar pull, normal force and sinkage would not vary once steady-state operation is reached. However, if one were to use the dynamic pressure-sinkage relationship shown in Equation (3) instead, then the drawbar pull, normal force and sinkage calculated by the analytical model would vary even after steady-state operation is reached, which more closely approximates data seen from experimental work Apostolopoulos et al. (2003); Arvidson et al. (2010); Irani et al. (2010a, 2011a) and shown in Figure 10. It should be pointed out that the dynamic model can be used for both smooth and grouser wheels operating in loose sandy soil. The following section examines the new parameters found in the dynamic pressure sinkage relationship.

1.1 Frequency ω

For a grouser wheel the frequency ω in Equation (3) is related to the spacing of the grouser blades and angular velocity of the wheel. Therefore, ω for a grouser wheel becomes:

$$\omega = \frac{\omega_w}{n_g} \tag{11}$$

where n_g is the number of grousers and ω_w is the angular velocity of the wheel in radians per second.

When a smooth wheel (no grousers) operates in sandy soil oscillations in the measured data are still observed. It is believed that the change in the local density around the wheel-soil interface is causing the oscillations in the data and repeatable ridges in the sand. Through empirical testing it was found that the frequency of the oscillations was linearly related to the slip ratio and independent of the normal load. As a result, the following empirical equation can be used to estimate the frequency as a function of the slip ratio i:

$$\omega = -36.9i + 36.5 \tag{12}$$

This equation was developed for a smooth rigid wheel of diameter .02 [m] and width 0.075[m] operating in sandy soil using a normal load of 14.9N (Irani et al. (2010a)), and a normal load of 47.7N was successfully used as a test case. A first order least-squares fit was performed for the 14.9N normal load data resulting in an R^2 value of 0.94. Equation (12) is unique unique to the test case for which it was developed. Therefore, with different terrains and/or wheel dimensions a new empirical equation must be found.

1.2 Amplitude A

There are two main factors that can contribute to the amplitude term A of Equation (3): a change in the local density near the wheel-soil interface and the added stress which grousers add to the interface. Thus, the amplitude term A can be written as:

$$A = A_\sigma + A_\gamma \tag{13}$$

where A_σ is related to the passive stresses which the terrain experiences due the added traction which grousers apply (for a smooth wheel A_σ would be zero) and A_γ is related to the local soil density change around the wheel caused by the soil deformation which occurs as the wheel travels through the terrain. The following sections will further explain and examine these two amplitude terms.

1.2.1 Passive Stresses; A_σ

Wong (2010) demonstrates how a grouser blade creates passive stresses to increase the tractive effort of a vehicle. The amplitude of the oscillations of the pressure-sinkage relationship could be a function of the passive stresses which are computed by Wong (2010):

$$\sigma_p = \gamma z N_\phi + q N_\phi + 2c\sqrt{N_\phi} \tag{14}$$

where the flow value N_ϕ is given by:

$$N_\phi = \tan^2\left(45^\circ + \frac{\phi}{2}\right) \tag{15}$$

In Equation (14), q is referred to as surcharge and is the additional pressure applied to the surface of the terrain from external sources. In a wheel-soil interaction, where the grouser of length h_b is exerting a passive stress on the soil, the normal stress $\sigma(\theta)$ from the smooth wheel section just ahead of the grouser would act as a surcharge. The length over which this surcharge contributes to the passive stresses is calculated by Wong (2001):

$$l_{qp} = \frac{h_b}{\tan\left(45^\circ - \frac{\phi}{2}\right)} \tag{16}$$

A passive stress acts in the same direction as the shear stress and, therefore, contributes additional components to the vertical and horizontal forces (see Equations (8) and (7)). Figure 3 shows the passive stress zones on the grouser face.

The formulation of the passive stresses shown in Equation (14) assumes the surcharge is uniform along the length l_{qp}. However, regardless of which pressure sinkage relationship one uses, at every depth along the wheel-soil interface there is a different stress state acting on the wheel because of the wheel's curvature. Thus, the surcharge acting on the grouser will not be uniform during the wheel-soil interaction. The mean pressure from the pressure-sinkage relationship acting along l_{qp} can be used to approximate the surcharge q. Also, when more than one grouser is in contact with the terrain, the mean of the passive stresses will be proportional to the amplitude term A_σ. Thus,

$$A_\sigma = k'_g \bar{\sigma_p} \tag{17}$$

where k'_g is an empirical dimensionless coefficient and $\bar{\sigma_p}$ is the mean of the passive stresses acting on the grouser blades which are in contact with the wheel.

The second amplitude term A_γ in Equation (13) is described in the following section.

1.2.2 Change in Local Density; A_γ

As an object travels through loose sandy soil there will be some form of deformation around the object. The deformation around the object will cause the granular particles to shift and fill in voids of the loosely pack structure of the initial terrain. This process can occur when a slipping wheel travels through loose sandy soil. If the local density increases around the wheel, then the strength of the sand would increase and the normal and shear stress which the wheel can exert on the soil (and, as a result, the vertical and horizontal forces acting on the wheel) will vary (Holtz et al. (1981)).

To account for this effect, amplitude term A_γ is related to the local change in the weight density of the soil around the wheel and the contact length l_c, which is the characteristic length describing the interface, as follows:

$$A_\gamma = k'_a l_c d\gamma \tag{18}$$

where k'_a is an empirical dimensionless coefficient and $d\gamma$ is the change in sand density which was taken as 10% of the initial undisturbed terrain. To determine the change in the density a soil sample was placed on a shaker table and excited at 30Hz and images where recorded so that a time-lapse analysis could be preformed. It was observed in time-lapse analysis that there was a 6.5% change in the density within 0.5 seconds and maximum of 14% change in density after 3 seconds. A value of 10% was used to approximate the density change as the wheel passed through the specific sand in this research. It should be pointed out that not all terrains will exhibit this drastic variation in the density. Before assigning a value of $d\gamma$ or k'_a one must first assess the degree to which the terrain experiences a change in density from small displacements or excitation. This assessment can come from laboratory testing with a shaker table or through *in-situ* testing with a compactor. Terrains which do not experience large variations in their density will have low $d\gamma$ and possibly a negligible k'_a. A k'_a of zero can be assigned if a slipping smooth-wheel does not produce any ridges in the terrain or in the sinkage, drawbar pull or normal force measurements. The contact length l_c is shown in Figure 2 and can be calculated by the following:

$$l_c = r\left(|\theta_f| + |\theta_r|\right) \tag{19}$$

where r is the radius of the wheel, and θ_f and θ_r are the corresponding entry and departure angles found from Equations (9) and (10), respectively. Substituting Equation (18), (17) and (13) into Equation (3) yields the final dynamic pressure-sinkage relationship for the terramechanic model:

$$p(z) = \left(ck'_c + \gamma b k'_\phi\right)\left(\frac{z}{b}\right)^n + \left(k'_g \bar{\sigma_p} + k'_a l_c d\gamma\right)\sin\left(\omega t + \Phi\right) \tag{20}$$

1.3 Implementation of the Dynamic Model

To implement the terramechanic model, an algorithm was constructed in MATLAB/Simulink as follows:

1. Model constants and constraints are inputted and an initial static sinkage is prescribed for $t = t_o$. The frequency ω is constant for the duration of test run and, therefore, Equation (12) or (11) can be calculated at this step.

2. Determine if any grousers are in contact with the soil and calculate θ_f and θ_r. Compute the mean value of the passive stress $\bar{\sigma_p}$ by first determining the surcharge q for each of the grousers in contact with the terrain in their respective locations so that A_σ can be computed.

3. Calculate A_γ from Equation (18) by first computing the contact length l_c from θ_f and θ_r. A in Equation (13) can now be applied to combine A_σ and A_γ.

4. Determine the normal stress $\sigma(\theta)$ and shear stress $\tau(\theta)$ and numerically integrate along the contact length to determine F_z and F_x using Equations (7) and (8).

5. Frictional damping F_f needs to be applied to the vertical direction as the terramechanic model does not account for any soil damping. For this work, viscous friction was assumed using a friction coefficient of 800 Ns/m. The sinkage acceleration can be determined from the sum of the forces in the vertical direction and then the sinkage acceleration can be integrated twice with respect to time such that an updated sinkage value is determined and can be used in the next time-step.

6. Return to Step 2 with the updated value of sinkage.

The algorithm presented above is shown in a flowchart found in Figure 4.

2 Case Studies

The following sections present a series of case studies to help demonstrate the usefulness and applicability of the dynamic pressure-sinkage relationship described by Equation (20). The first case study examines how smooth wheels mounted on a 4-wheeled micro rover testbed interact with sandy soil at different slip ratios as the rover navigates an incline. The second case study uses passive stress theory to simulate a wheel grouser interacting with the soil. The third case study investigates the influence of grouser height on the wheel-soil interaction at different slip ratios using measurements from a single wheel testbed. The fourth case study also uses a single wheel testbed and focuses on how wheels with different number of grousers interact with sandy soil at different slip ratios.

2.1 Case Study #1: Smooth Wheel Rover Tests

The single-wheel testbed research performed by Apostolopoulos et al. (2003) used 15.2kg inflatable wheels with a radius of 70cm along the compressed axis, and a contact width of approximately 1m. Apostolopoulos et al. mentioned that repeatable ridges 5cm wide and 3cm tall were found in the wheel track as it operated in sandy soil. Ishigami's PhD thesis (2008) presented images showing similar repeating ridges in the track of a smooth rigid wheel operating in a Lunar simulant or Toyoura Sand. Ishigamis work did not mention or focus on these ridges in the wheel track. As previously mentioned, Irani et al. (2010a) has developed a dynamic pressure-sinkage model after noticing ridges in the track of a smooth wheel operating in sandy soil. However, all of the documented cases found in the literature come from tests preformed on single-wheel testbeds and, therefore, the question must be answered: Are these ridges an artifact of the single-wheel testbed or are the ridges a natural phenomena that occurs with a real lightweight mobile robot operating in sandy soil?

To answer this question a four-wheel micro rover having 100mm diameter smooth wheels was constructed and tested in sandy soil. The rear wheels were driven through a 505.9:1 geartrain while the front wheels were free to rotate. Given the dynamic pressure-sinkage relationship presented in Section 1, it was hypothesized that the rear wheels, when slipping, would produce repeatable ridges, and that the front wheel would leave a smooth track since their drawbar pull would be negative. A tachometer was used to determine the angular velocity of the wheels

and a potentiometer was used to record the linear translation of the 1.6kg vehicle. The rear wheels rotated at an average speed of 9.5rpm with a standard deviation of 0.21.

To achieve a repeatable and consistent slipping condition, hill climbing tests were carried out at $3.5°, 5°$ and $6°$ (maximum inclination which the rover could climb) which corresponded to rear-wheel slip ratios of 0.8, 0.95 and 0.96, respectively. Incline angles between $0°$ and $3.5°$ did not produce consistent or repeatable slip conditions. The reason for the irregular results at low inclines is likely from the initial conditions of the test sand where, before each test, the sand was manually mixed and leveled with a scraper tool. It is likely that the local density was not perfectly uniform after this manual preparation process and, therefore, when the micro rover traversed the terrain, any small variations in the terrain influenced the mobility of the vehicle. Once the slip ratio increased to 0.8, the micro rover's rear wheels produced consistent and repeatable ridges in the sand as predicted.

The results of these tests can be seen in Figure 5 which shows the micro rover and its tracks with the ridges at the various slip ratios. Also, as predicted and shown in Figure 5, the un-powered front wheel produced a smooth flat track. Figure 6 shows a selection of the tracks from the rear wheels for the inclines tested and, in this figure, heavy lines have been digitally superimposed to help the reader identify the ridges. When a linear least squares curve fit was performed on the three slip ratios tested, a linear relationship was found. This linear result from the micro rover case study confirms earlier published work of Irani et al. (2010a) where it was shown that there is linear relationship between the frequency of the oscillations and the slip ratio when a smooth wheel was tested on a single-wheel testbed (SWTB).

The results of this case study also indicate that the dynamic pressure-sinkage model described by Equation (20) should only be used when positive drawbar pull is established at a sustained slipping state. The case study also shows that the ridges in the sand are not an artifact of the single-wheel testbed — they are, in fact, a natural phenomena that occurs when a lightweight mobile robot operates in sandy soil. It is believed that the ridges are caused be the local change in density on the wheel-soil interface (Irani et al. (2011a). Therefore, if a terrain does not experience a density variation when a smooth slipping wheel passes though it, a k'_a of zero can be assigned to that wheel-soil interaction.

The micro rover was tested with smooth wheels; however, most wheels have grousers to aid their tractive effort.

2.2 Case Study #2: Passive Stress Theory – Dynamic Effect of Grousers

A theoretical case study was performed to examine how passive stresses from a grouser on a rotating wheel affect the resulting normal and shear stress acting on the wheel. In this case study a wheel was simulated which:

- was 20 cm in diameter
- operated at a slip ratio of 0.35 with a sinkage of 5cm while η is 0.95
- had grousers that were 15mm long and 3mm thick

The results of this theoretical case study are shown in Figure 8 which plots the corresponding normal and shear stress as a function of angular position along the wheel as the grousers travel through the terrain in sequential time steps. As shown in Figure 8, when $t = t_o$ the grouser is located at $-40°$ and then, at the next time-step, $(t = t_1)$ the grouser is located at $-60°$. One will notice that, although the passive stresses from a grouser have little effect on the normal stress, the passive stresses significantly affect the shear stress (up to an order of magnitude larger than the nominal shear stress). The grouser thickness only contributes about 15% to the normal stress when compared to the overall magnitude of the normal stress and only acts over the width of the grouser. Furthermore, it can be seen that the passive stress contribution of an individual grouser varies as it moves through the terrain, and variations in the resulting normal and shear stress distribution around the wheel cause variations in the resulting forces acting on the wheel. As a result of this case study it becomes clear that passive stresses should be incorporated into the pressure-sinkage relationship.

2.3 Case Study #3: SWTB Experiments – Dynamic Effect of Grousers

A series of experiments were carried out on a single-wheel testbed (SWTB) using a wheel with grousers to study the ability of the dynamic pressure sinkage model described by Equation (20) (Irani et al. (2011a)) to predict the normal force, drawbar pull and sinkage for different slip ratios and grouser geometry. Figure 9 shows the experimental setup of the SWTB used during testing.

A wheel with 16, 23mm long grousers operating at a slip ratio of 0.50 and a normal load of 15N was used as the sole tuning case for the terramechanic model described in Section 1. The parameters used in the model and their values can be found in Table 1. The shear deformation modulus K and ϕ can be found through triaxial, ring shear or shear box laboratory testing. Typically, in dry sand the cohesion c is very low and can be found through a ring shear or shear box laboratory testing (Wong (2010) and Holtz et al. (1981)). In the case of the sand used in this research the cohesion was below the sensitivity of the equipment and therefore it was taken as zero for this work. Taking sand as cohesionless is not uncommon in soil mechanics (Holtz et al. (1981)). The initial weight density of the sand was measured in the laboratory by measuring the weight of a known volume of the sand. The sinkage exponent n is taken as 1 for dry sands (Wong (2010)). The non-dimensional coefficient k'_c was set to zero as suggested by Wong (2001; 2010). The value of η has said to be a function of the wheel's geometry, soil ratio and the soil conditions (Ishigami et al. (2007)). If one has definite measurements for η in various scenarios, those values of η should be used. The rear of wheel sinkage relationship η was visually inspected to be 1.35 for the test case and used for all other cases as the predictive abilities of the model are examined in this work. Through experimental experience the value of 1.35 is not unreasonable for a variety of scenarios with the experimental wheels and sand used in this work. The only parameter left in the classic terramechanic model is the non-dimensional coefficient k'_ϕ. This parameter was manually tuned to a value of 20. The tuning was done by slowly increasing the value of k'_ϕ until the means of the measured data were reasonably represented by the simulation. Once the classic model was tuned, values for k'_g and k'_a of the new dynamic model need to be determined. For a

grouser wheel the contribution of the passive stresses would dominate the tractive effort and therefore, a ratio of 2:1 was used for $k'_g : k'_a$. To manually tune the model a value of k'_g was set and k'_a was calculated. The value of k'_g was then slowly increased and the resulting amplitude of the oscillations were observed in the simulated results until a reasonable approximation was found for the experimental results for the sole tuning case.

The parameters in Table 1 were held constant throughout all of the simulations carried out for this case study and the next two case studies. Figure 10 plots the sinkage, drawbar pull and normal load as a function time and overlays experimental results with the dynamic pressure-sinkage model described by Equation (20) and Bekker's traditional terramechanic model. Bekker's terramechanic model was able to reasonably model the mean sinkage and normal force; however, it under predicted the drawbar pull by 5N for this case. This under prediction can be attributed to the fact that Bekker's traditional terramechanics model was originally developed for wheels larger than 50 cm (Bekker (1969); Wong (2001); Meirion-Griffith and Spenko (2011)). It has been recently shown by Meirion-Griffith and Spenko (2011) that smaller wheels tend to experience greater sinkage than the predicted values from Bekker's model which, in turn, can lead to larger rolling resistances and reduced tractive performance. As a result, drawbar pull would be underpredicted as confirmed by Figure 10. One will notice that the dynamic pressure-sinkage model oscillates about the mean values predicted by Bekker's terramechanic model as expected and accurately predicts the amplitudes and frequencies of the oscillations observed in the measured data. It should be noted that, although any adjustments or improvements to the mean values in Figure 10 using correction factors such as those discussed by Meirion-Griffith and Spenko (2011) would require re-tuning of the dynamic pressure-sinkage relationship, the resulting accuracy of the predicted amplitudes and frequencies of the oscillations would be maintained.

To further validated the predictive capabilities of the model, comparisons for slip ratios of 0.15, 0.25, 0.35 and 0.75 can be seen in Figure 11, which presents the data as mean-adjusted plots during steady-state operation so that the oscillations and contribution of the dynamic pressure-sinkage relationship described by Equation (20) be can be easily compared. The model parameters used for these cases were the same as those used to manually tune the model (Table 1). The gradual entrance and exit of a grouser from the terrain is not considered in this work and one will notice small discontinuities in the simulated data from the dynamic pressure-sinkage model in the presented data. The root mean squared (RMS) data comparing the simulated and experimental work is presented in Table 2 along with the absolute difference or delta between these two calculations. The RMS values were taken from the mean adjusted comparisons for the time periods shown in Figures 10 and 11. The RMS values indicate reasonable and consistent results when compared to the time history results of Figures 10 and 11.

Figure 11 shows that the dynamic model is able to accurately predict the oscillations in the sinkage, drawbar pull and normal force for all cases except for the 0.75 slip ratio case. At this high slip ratio the wheel is excavating the terrain and the sinkage becomes smoother. When the excavation increases one will also notice that the RMS delta (difference) values (Table 2) increase for all three measurements. When examining the normal load RMS delta for the 0.75 slip ratio

case, the model is over predicting the amplitude and the resulting RMS delta is 1.338. A possible explanation for this reduction in the experimental oscillation amplitude is that, at such high slip ratios, the terrain does not come to rest before the next grouser comes into contact with it resulting in a more continuous flow of sand material. Such as fluidization, which can occur when a granular material is excited by small displacements through vibration or other means, cause the macroscopic property of the granular system to change from a solid to a fluid Jaeger and Nagel (1992). This fluidization phenomena is not accounted for in the current terramechanic model.

The next case study investigates the ability of the new dynamic model to predict oscillations in the sinkage, drawbar pull and normal force when the grouser length is reduced from 23mm to 10mm.

2.4 Case Study #4: SWTB Experiments – Grouser Length

Building on the previous case study, SWTB experiments were carried out using a 16 grouser wheel which had the length of each grouser reduced from 23mm to 10mm. Figure 13 plots the resulting mean-adjusted experimental and simulated values for sinkage, drawbar pull and normal force as a function of time for slip ratios of 0.25, 0.35, 0.50 and 0.60. The values used for this case study were, again, kept the same as those used to originally tune the model (Table 1). For this case study, Table 3 presents the RMS data for the experimental and simulated data. The table also presents the difference or delta between these two calculations. The RMS values were taken from the mean adjusted comparisons for the time periods shown in Figure 13 and indicate reasonable and consistent results when compared to the time history data of Figure 13.

One can see from Figure 13 that, for the 0.25 and 0.35 slip ratio cases, the oscillations in all of the measured data is accurately predicted by the model. As observed in the previous section, at the higher slip ratios, particularly 0.60, the model begins to lose its predictive capability for the oscillations in the sinkage. This result is expected based on the previous Case Study. As the wheel begins to spin for longer periods of time in the same location, the wheel appears to continuously excavate the surrounding terrain. Since the wheel lacks appreciable forward movement into undisturbed terrain, the grousers cause the sand in the vicinity of the wheel to be in constant motion. This fluidization phenomena occurring with high-slip conditions is not accounted for in the dynamic pressure-sinkage relationship.

2.5 Case Study #5: SWTB – Grouser Number

For this case study the number of grousers, each 10mm long, was increased from 16 to 32, and SWTB experiments and corresponding model simulations were carried out. Figure 12 show the resulting mean-adjusted overlay of experimental and simulated sinkage, drawbar pull and normal force plotted as a function of time for slip ratios of 0.25, 0.50, 0.60 and 0.75. The model parameters used for this case study were again set using the original tuning case (Table 1). One will notice from Figure 12 that all of the experimental sinkage results, including those at the lowest slip ratio tested, did not present noticeable oscillations. This observation, given

the resulting increase in flow of sand grains caused by a doubling of the number of grousers, can likely be attributed to the same fluidization phenomena which occurred in the previous two test cases. When examining the drawbar pull results in Figure 12 one can see that the results are reasonable for slip ratios of 0.25, 0.50 and 0.60; however, at a slip ratio of 0.75 the oscillations become less significant in all three measured signals — again, likely due to fluidization as the sand grains experience a constant flow at these higher slip ratios.

The RMS data comparing the simulated and experimental work is presented in Table 4. The RMS values show a large over prediction from the model, especially in the normal force results where the minimum and maximum deltas are 1.778 and 3.187, respectfully. One will notice that the delta RMS values of the sinkage results are very small, suggesting that the model is accurately predicting the amplitude of the oscillations. However, examining the time history data in Figure 12 one will see that there are no oscillations in the sinkage measurements. Therefore, examining only the RMS values as a measure of accuracy can be misleading. If one examines Figure 12, the experimental data has some natural variation or drift for all slip ratios during the time period shown in the figure. The amplitude of the drift is very close to the amplitude of the model-predicted oscillations. Since RMS calculations are independent of phase and frequency, one cannot rely solely on the delta RMS data to conclude if the results are accurate, reasonable or valid. To correctly interpret the RMS results, one must also examine the time history response to conclude if excessive excavation is occurring.

3 Conclusions

As a result of the case studies presented in this work, the authors have shown that the dynamic pressure-sinkage model described by Irani et al. (2010a, 2011a) should only be implemented when there is sustained slippage and positive drawbar pull for smooth wheel cases. Case studies which varied the number and length of the grousers on a wheel demonstrated that the model is able to reasonably capture and predict the dynamic oscillations observed in the drawbar pull and normal force measurements using only one tuning condition (16, 23mm long grousers operating at a slip ratio of 0.50 and a normal load of 15N). Under high-slip conditions or when the number of grousers on a wheel is relatively high, there appears to be an unaccounted for fluidization phenomena which reduces the amplitude of the observed oscillations in the sinkage. Also, RMS data should be used in conjunction with time history data to ensure the numeric quantification is appropriate and meaningful.

Further work needs to be carried out to explore the full potential and limitations of the dynamic pressure-sinkage relationship, such as side slip effects, terrain variations and its application in terrain parameter estimation.

FIGURES

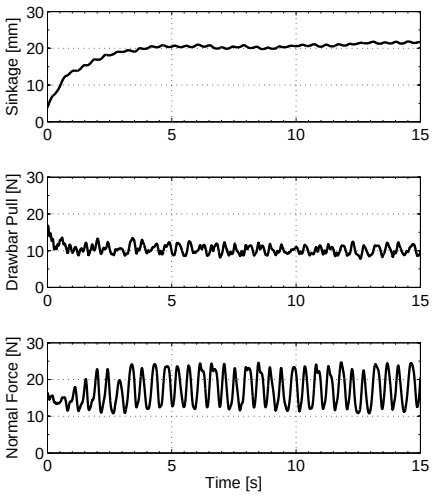

Figure 1 Experimental data of a rigid wheel with 16, 23mm long grousers, operating at 0.50 slip and a 15N normal load

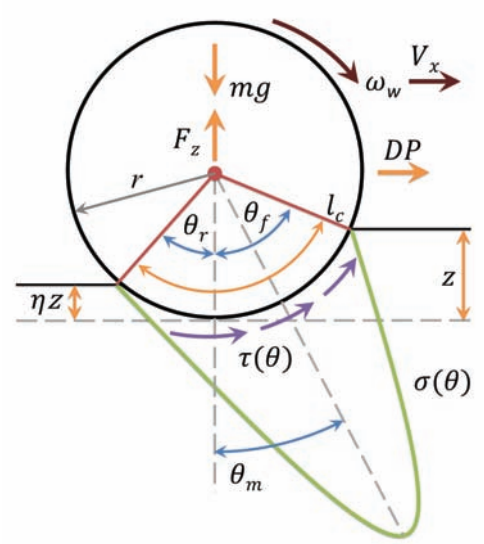

Figure 2 Forces and stress acting on a wheel which a typical terramechanic model calculates

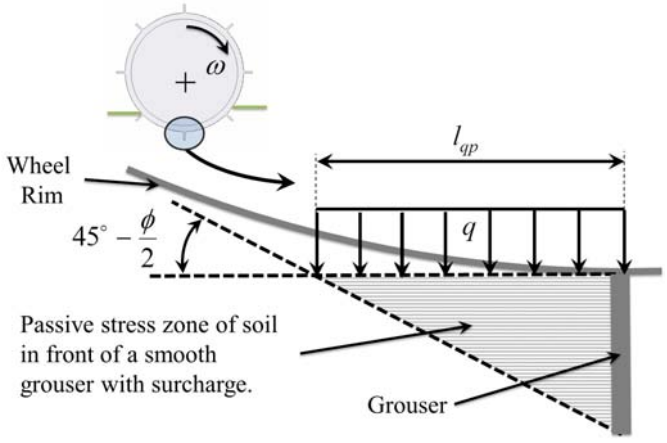

Figure 3 Active and Passive stress zones on a wheel when grousers are present

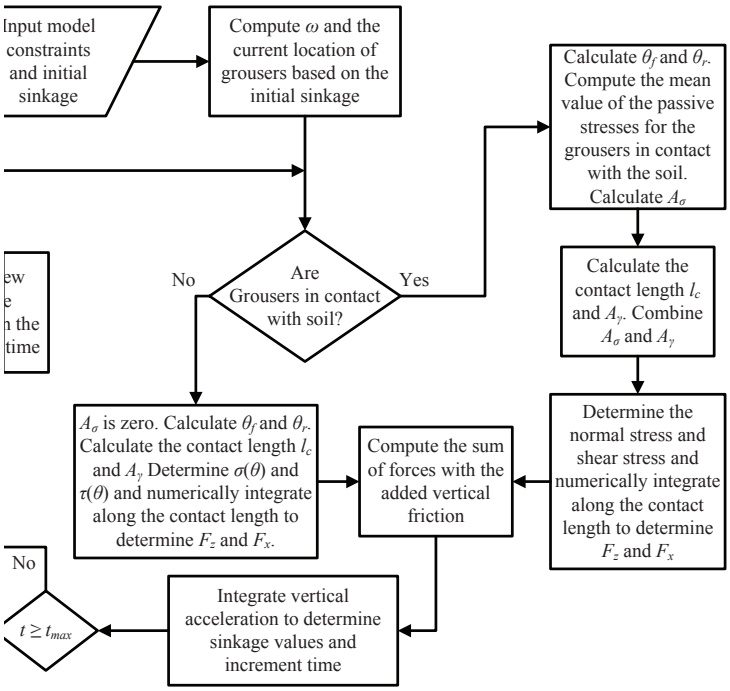

Figure 4 Flow chart of the algorithm implemented in MATLAB/Simulink

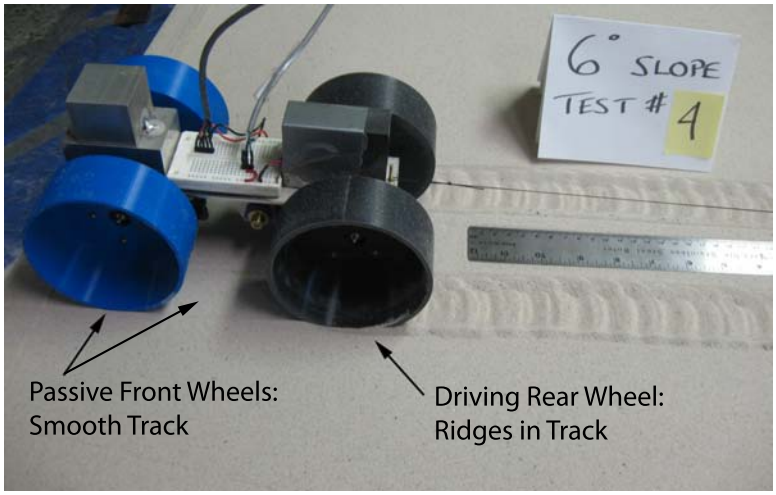

Figure 5 Micro rover at the end of a 6° slope climb

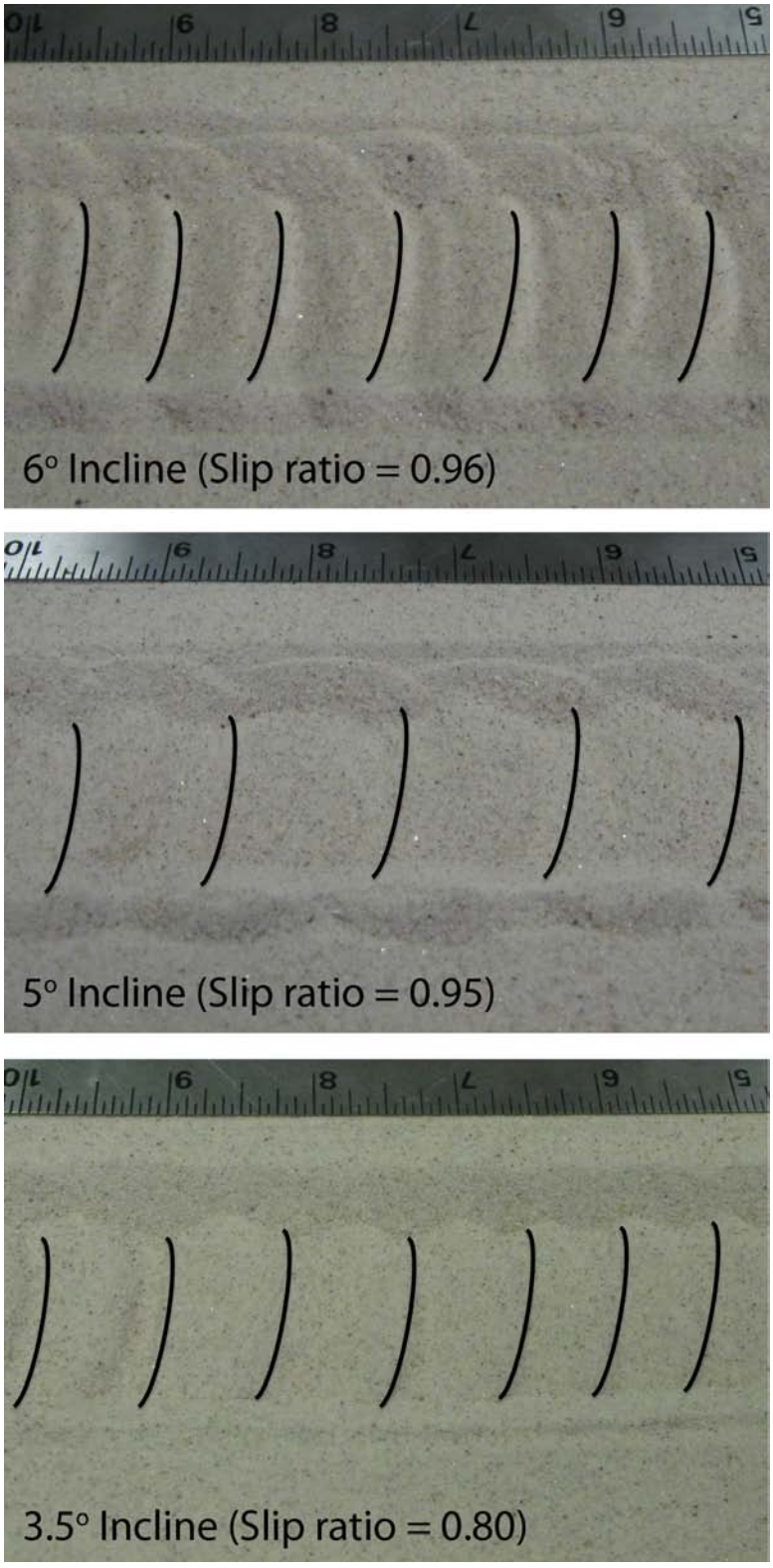

Figure 6 Tracks from the rear wheels of the micro rover

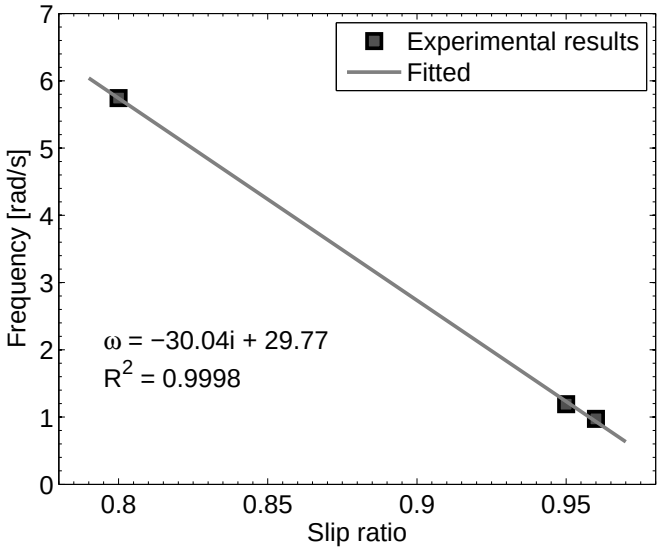

Figure 7 Ripple Frequency vs slip ratio

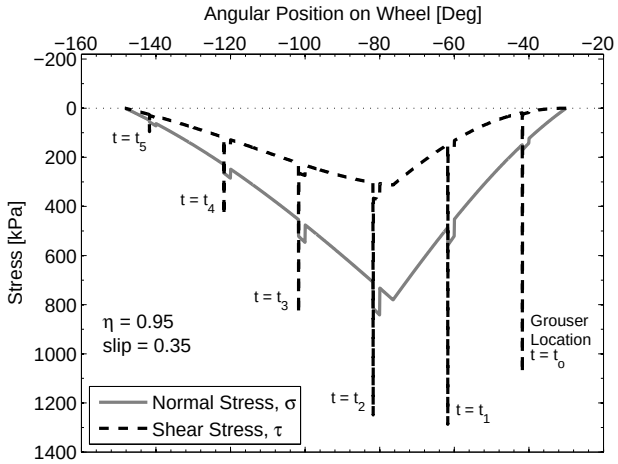

Figure 8 Normal and shear stress along the face of the wheel with active and passive stress added to the shear stress

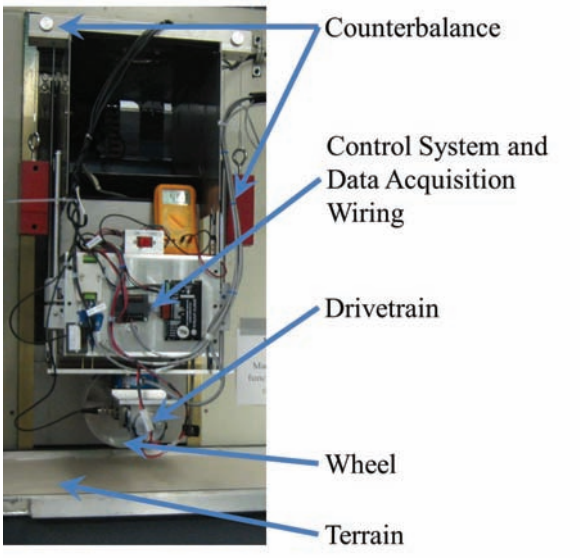

Figure 9 Experimental equipment: Single wheel testbed (SWTB)

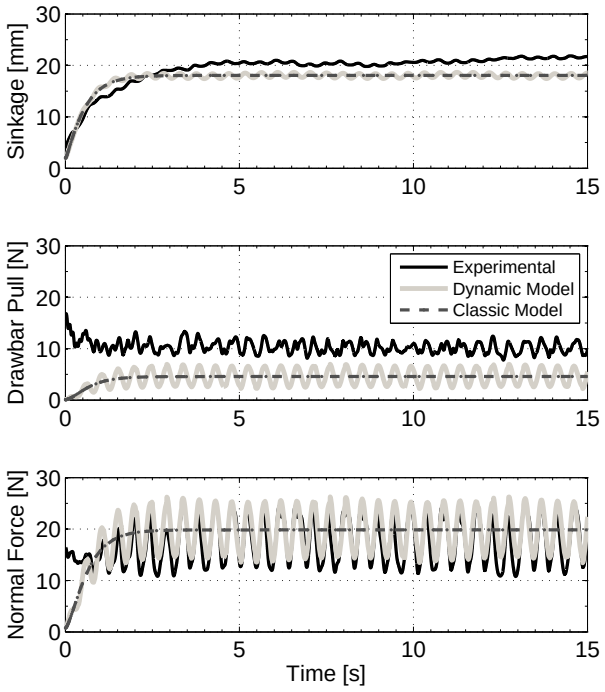

Figure 10 Overlay of experimental data with the dynamic and classic models for a rigid wheel with 16, 23mm long grousers, operating at 0.50 slip and a 15N normal load

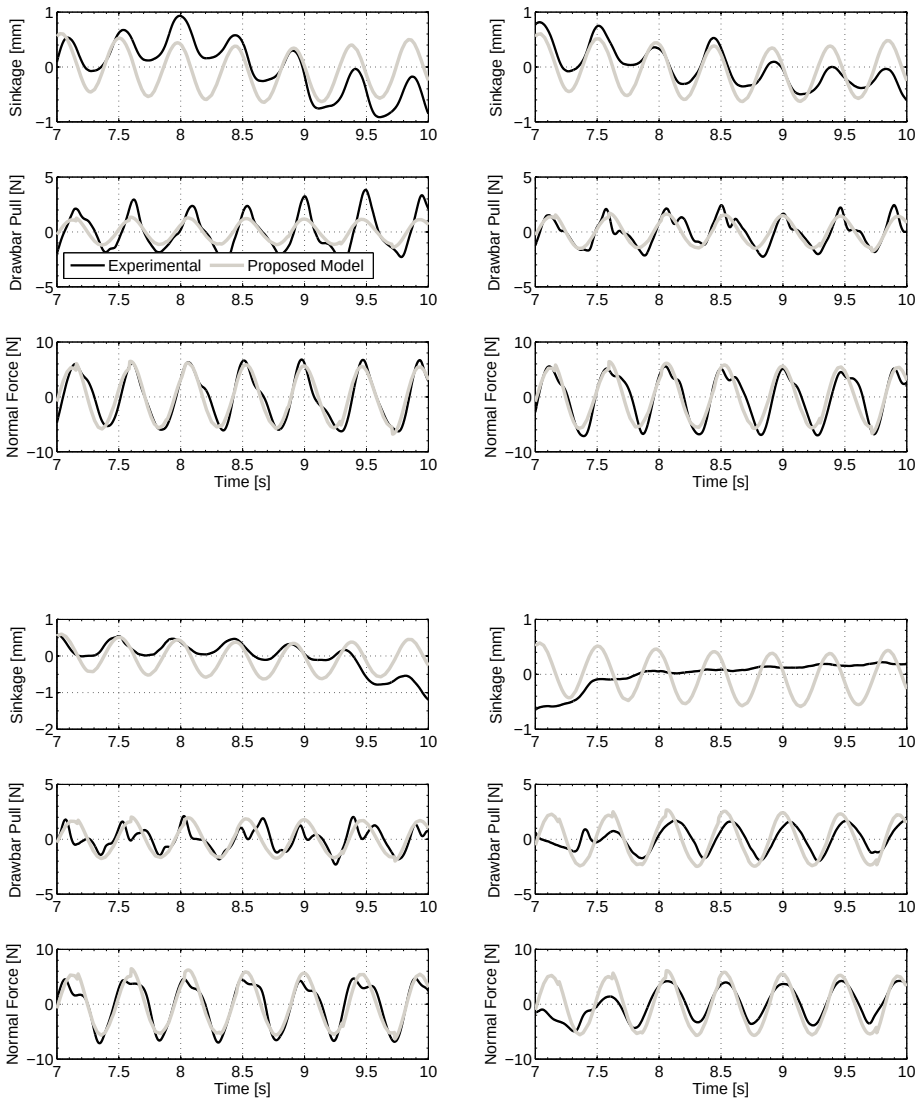

Figure 11 Mean adjusted simulation data of a rigid wheel with 16, 23mm long grousers, operating with a 15N normal load overlayed with experimental data. Top Left) 0.15 slip ratio; Top Right) 0.25 slip ratio Bottom Left) 0.35 slip ratio; Bottom Right) 0.75 slip ratio

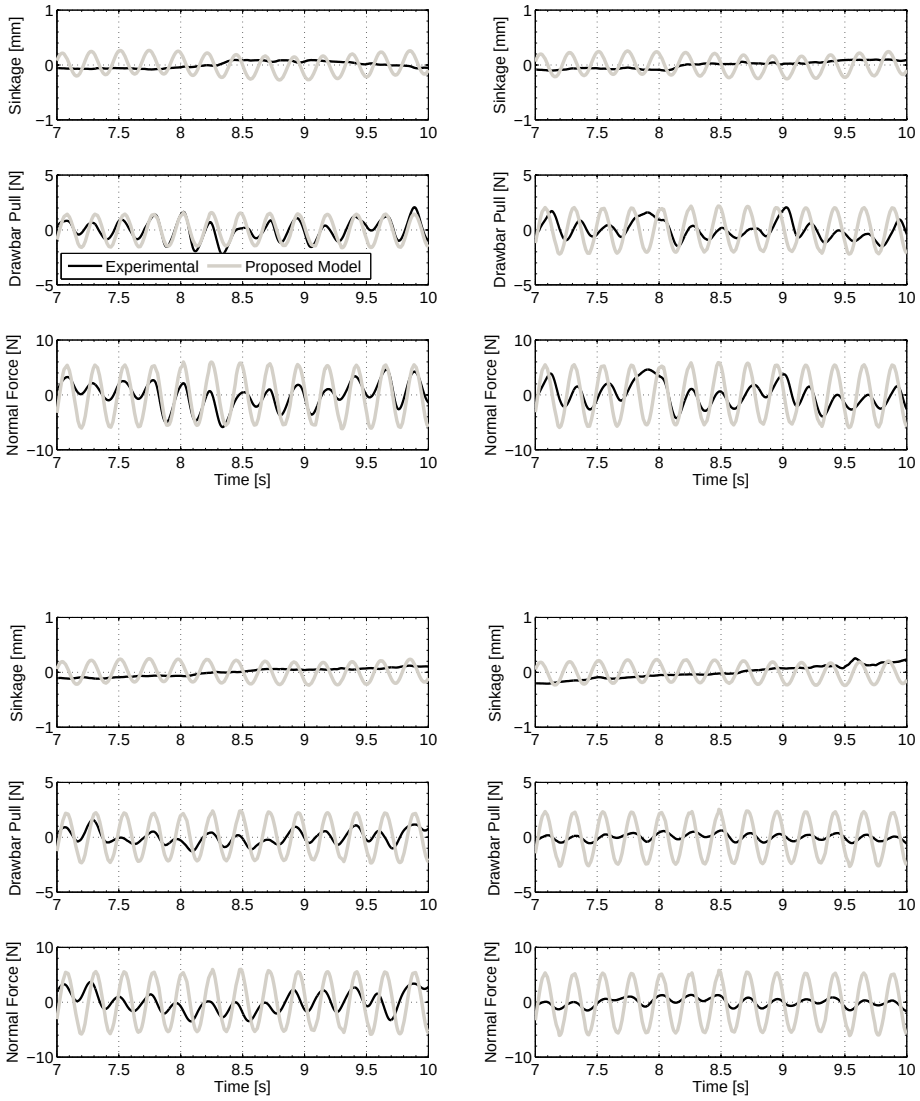

Figure 12 Mean adjusted simulation data of a rigid wheel with 32, 20mm long grousers, operating with a 15N normal load overlayed with experimental data. Top Left) 0.25 slip ratio; Top Right) 0.50 slip ratio Bottom Left) 0.60 slip ratio; Bottom Right) 0.75 slip ratio

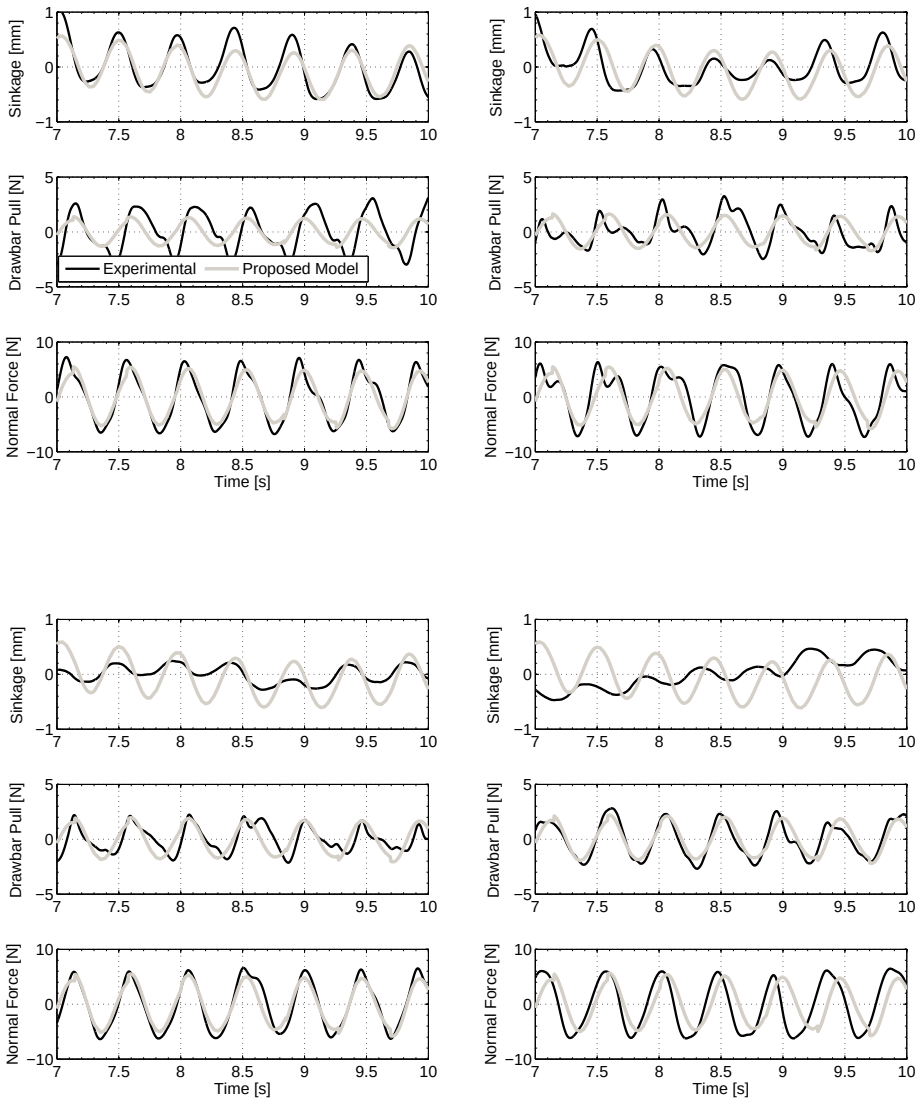

Figure 13 Mean adjusted simulation data of a rigid wheel with 16, 10mm long grousers, operating with a 15N normal load overlayed with experimental data. Top Left) 0.25 slip ratio; Top Right) 0.35 slip ratio Bottom Left) 0.50 slip ratio; Bottom Right) 0.60 slip ratio

TABLES

Table 1 Summary of Parameters

Parameter	Value	Unit	Comments
k'_c	0	–	Dimensionless cohesive modulus
k'_ϕ	20	–	Dimensionless frictional modulus
K	0.036	m	Shear deformation modulus
n	1	–	Sinkage exponent
γ	13734	N/m^3	Soil weight density
$d\gamma$	$0.1 \times \gamma$	N/m^3	Change in soil weight density
r	0.1	m	Radius of wheel
b	0.075	m	Width of wheel
η	1.35	–	Rear of wheel sinkage relationship
ϕ	28	deg	Internal angle of friction
c	0	kPa	Soil cohesion
C_f	800	Ns/m	Viscous friction coefficient
k'_g	0.1	–	Dimensionless grouser amplitude coefficient
k'_a	0.05	–	Dimensionless density amplitude coefficient

Table 2 RMS Data for Case Study #3

Sinkage

Slip Ratio	RMS Experimental	RMS Proposed Model	$\|\Delta\|$ Difference
.15	0.478	0.339	0.139
.25	0.264	0.336	0.072
.35	0.317	0.337	0.020
.50[1]	0.257	0.333	0.076
.75*	0.171	0.330	0.159

Drawbar Pull

Slip Ratio	RMS Experimental	RMS Proposed Model	$\|\Delta\|$ Difference
.15	1.679	0.896	0.783
.25	1.196	1.129	0.066
.35	0.957	1.330	0.374
.50[1]	1.003	1.539	0.536
.75	1.099	1.807	0.708

Normal Force

Slip Ratio	RMS Experimental	RMS Proposed Model	$\|\Delta\|$ Difference
.15	4.187	4.342	0.155
.25	4.232	4.271	0.039
.35	3.811	4.254	0.443
.50[1]	4.094	4.151	0.57
.75	2.792	4.130	1.338

[1] Denotes the slip ratio which the model was tuned with

* Denotes measurements where the oscillations were diminished due to an un-modeled phenomena

Table 3 RMS Data for Case Study #4

Sinkage

Slip Ratio	RMS Experimental	RMS Proposed Model	$\|\Delta\|$ Difference
.25	0.419	0.312	0.107
.35	0.282	0.311	0.029
.50	0.150	0.308	0.158
.60	0.259	0.305	0.047

Drawbar Pull

Slip Ratio	RMS Experimental	RMS Proposed Model	$\|\Delta\|$ Difference
.25	1.691	0.948	0.743
.35	1.301	1.125	0.177
.50	1.145	1.340	0.195
.60	1.573	1.460	0.115

Normal Force

Slip Ratio	RMS Experimental	RMS Proposed Model	$\|\Delta\|$ Difference
.25	4.381	3.770	0.611
.35	4.240	3.759	0.481
.50	4.188	3.754	0.434
.60	4.461	3.764	0.697

Table 4 RMS Data for Case Study #5

Sinkage

Slip Ratio	RMS Experimental	RMS Proposed Model	$\|\Delta\|$ Difference
.25*	0.060	0.158	0.099
.35*	0.065	0.152	0.087
.50*	0.072	0.149	0.077
.75*	0.116	0.149	0.032

Drawbar Pull

Slip Ratio	RMS Experimental	RMS Proposed Model	$\|\Delta\|$ Difference
.25	0.862	1.062	0.200
.35	0.794	1.474	0.680
.50	0.615	1.581	0.966
.75	0.285	1.708	1.423

Normal Force

Slip Ratio	RMS Experimental	RMS Proposed Model	$\|\Delta\|$ Difference
.25	2.237	4.015	1.778
.35	2.082	3.978	1.896
.50	1.790	3.940	2.150
.75	0.716	3.903	3.187

* Denotes measurements where the oscillations were diminished due to an un-modeled phenomena

References

Azimi A., Hirschkorn M., Ghotbi B., Kovecses J., Angeles J., Radziszewski P., Teichmann M., Courchesne M., and Gonthier Y. (2010) Simulation-based rover performance evaluation and effects of terrain modelling, *In CASI Astronautics Conference ASTRO 2010*, May 4-6 2010.

Apostolopoulos D. , Wagner M., Heys S. and J. Teza. (2003) Results of the inflatable robotic rover testbed. Technical Report CMU-RI-TR-03-18, Carnegie Mellon University, June 2003.

Arvidson, R.E. and Bell III, J.F. and Bellutta, P. and Cabrol, N.A. and Catalano, J.G. and Cohen, J. and Crumpler, L.S. and Des Marais, D.J. and Estlin, T.A. and Farrand, W.H. and others (2010). Spirit Mars Rover Mission: Overview and selected results from the northern Home Plate Winter Haven to the side of Scamander crater. *J. Geophys. Res*, 115, 2010.

M. G. Bekker (1969). Introduction to terrain-vehicle systems. University of Michigan Press, Ann Arbor.

Holtz R.D. and Kovacs W.D. (1981). An introduction to geotechnical engineering, volume 733. Prentice-Hall.

Ishigami G., Miwa A., Nagatani K., and Yoshida K. (2007). Terramechanics-based model for steering maneuver of planetary exploration rovers on loose soil. *Journal of Field Robotics*, 24(3):233250.

Ishigami G. Terramechanics-based Analysis and Control for Lunar/ Planetary Exploration Robots. Phd Thesis, Tohoku University, Department of Aerospace Engineering, March 2008.

Jaeger H.M. and Nagel S.R. (1992). Physics of the granular state. *Science*, 255(5051):1523.

Karafiath L.L. and Nowatzki E.A. (1978). Soil Mechanics for Off-Road Vehicle Engineering. Clausthal Germany: Trans Tech Publications.

Lyasko M. (2010). LSA model for sinkage predictions. *Journal of Terramechanics*, 47(1):1-19.

Meirion-Griffith G. and Spenko M. (2011). A modified pressure sinkage model for small, rigid wheels on deformable terrains. *Journal of Terramechanics*, 48(2):149 155.

Irani R., Bauer R., Warkentin A. (2011a). A dynamic terramechanic model for small lightweight vehicles with rigid wheels and grousers operating in sandy soil. *Journal of Terramechanics*, 48(2): 307-318.

Irani R., Bauer R., Warkentin A. (2011). Dynamic terramechanic model for grouser wheels on a planetary rover in sandy soil. *In CANCAM, 2011.* Vancouver, British Columbia.

Irani R., Bauer R., Warkentin A. (2010b). Modelling a single-wheel testbed for planetary rover applications. *In Third Annual Dynamic Systems and Control Conference, 2010.* Cambridge, Massachusetts.

Irani R., Bauer R., Warkentin A. (2010a). Design of a single-wheel testbed and preliminary results for planetary rover applications. *In The Canadian Society for Mechanical Engineering Forum 2010.* Victoria, British Columbia.

Reece A.R. Principles of soilvehicle mechanics. *Proceedings of the Institution of Mechanical Engineers, Automobile Division*, 180(1965):4566.

Wong J. Y. (2001). Theory of ground vehicles. John Wiley, New York.

Wong J.Y. (2010). Terramechanics and Off-Road Vehicles. Butterworth-Heinemann, 2 edition.

Hanamoto B. and Janosi J. (1961). The analytical determination of drawbar pull as a function of slip for tracked vehicle in deformable soils. *In 1st Int. Conf. on Terrain-Vehicle Systems*, Torino, Italy.